Journal of Sound and Vibration 381 (2016) 101–120

Contents lists available at ScienceDirect

Journal of Sound and Vibration

journal homepage: www.elsevier.com/locate/jsvi

# Aeroacoustics research in Europe: The CEAS-ASC report on 2015 highlights

Ondřej Jiříček

*Czech Technical University in Prague, Faculty of Electrical Engineering, Technicka 2, 166 27 Prague, Czech Republic*

ARTICLE INFO

*Article history:*
Received 16 May 2016
Accepted 20 June 2016
Handling Editor: P. Joseph
Available online 12 July 2016

*Keywords:*
Aeroacoustics
Noise
Numerical modeling

ABSTRACT

The Council of European Aerospace Societies (CEAS) Aeroacoustics Specialists Committee (ASC) supports and promotes the interests of the scientific and industrial aeroacoustics community on the European scale, and European aeronautics activities internationally. Each year, the committee highlights several of the research and development projects in Europe. This paper is the 2015 issue of this collection of Aeroacoustic Highlights, compiled from contributions submitted to the CEAS-ASC.

The contributions are classified in different topics; the first categories being related to specific aeroacoustic challenges (airframe noise, fan and jet noise, helicopter noise, aircraft interior noise), while the two last sections are devoted respectively to recent improvements and emerging techniques and to general advances in aeroacoustics. Furthermore, a concise summary of the CEAS-ASC workshop "Broadband noise of rotors and airframes" held in La Rochelle, France, in September 2015 is included in this report.



## 1. Introduction

The CEAS-ASC each year provides a report summarizing significant advances in aeroacoustic research fields. The present paper corresponds to the 2015 edition of this report. As for previous editions, it would be impossible to give a detailed view of the scientific activity in each research topic, and the present paper focuses on innovative advances and findings from accomplished projects funded by European, industrial or national programmes. The paper is organized as a collection of contributions, divided into sections corresponding to the main topics of research in 2015.

## 2. CEAS-ASC Workshop

The 19th CEAS-ASC Workshop was held in Espace Encan, La Rochelle, France, on September 23–25, 2015, in conjunction with ANERS 2015 (Aircraft Noise and Emissions Reduction Symposium) and the fifth Scientific Workshop of X-NOISE EV. Organized by Denis Gély (ONERA, France), the workshop title was "Broadband Noise of Rotors and Airframes". The workshop had five keynote speakers:

- Lars Enghardt (DLR, Germany) on "FLOCON: Adaptive and Passive Flow Control for Fan Broadband Noise Reduction. Selected Final Results".

*E-mail address:* jiricek@fel.cvut.cz

http://dx.doi.org/10.1016/j.jsv.2016.06.029
0022-460X/

- Mike Jones (NASA Langley RC, USA) on “NASA Langley Activities on Broadband Fan Noise Reduction via Novel Liner Technologies”.
- Thomas Nodé-Langlois (Airbus, France) on “Stakes and State of the Art of Aircraft Broadband Noise Sources Modeling” (presented by N. Molin and S. Lidoine).
- Matthieu Fiack (Snecma, France) and Nick Humphreys (Rolls-Royce, UK) on “Broadband Noise: A Key Driver for Future Power-plant Systems”.
- Eric Manoha (ONERA, France) on “Landing Gear Broadband Noise Prediction: What is the Best Method?”.

There were 24 contribution papers in five sessions presented to 68 participants from 16 countries. At the beginning, Jeremy Astley reminded the audience of Geoffrey M. Lilley (equation of jet noise) who passed away recently.

## 3. Airframe noise

### 3.1. Aerofoil–turbulence interaction noise reductions by using wavy leading edges

In recent years at the University of Southampton, progress has been made to investigate and understand the effects of wavy leading edge (WLE) serrations on the reduction of aerofoil–turbulence interaction noise. Experimental measurements were performed to find the relationships between the geometric changes (serration amplitude and wavelength) and the level of noise reduction relative to the baseline case with a straight leading edge (SLE) [33]. It was found that the serration amplitude is the major parameter that controls the level of noise reduction, which confirmed the findings of an earlier study by Lau et al. [29]. The sound power spectra showed that the noise reduction begins to take place at a frequency where the corresponding hydrodynamic wavelength is around twice the serration length. In the meantime, high-resolution computational simulations were also performed to understand the noise reduction mechanisms associated with the source characteristics at the aerofoil surface (Fig. 1) [26]. The numerical results revealed two major mechanisms of noise reduction [27]. The first mechanism discovered is “source cut-off” effect. The oblique part of the WLE generates substantially weakened source power, which effectively leaves the peak and root areas as isolated discrete source spots (Fig. 2). The second mechanism is “source phase-interference” effect. It was found that the WLE geometry produces an increased level of phase interference (more out-of-phase frequency components) in the source signals between the peak and the rest of the WLE (Fig. 3).

*Written by Jae Wook Kim* (*j.w.kim@soton.ac.uk*), *Aerodynamics & Flight Mechanics Research Group, University of Southampton, United Kingdom.*

### 3.2. The pseudo equivalent deterministic excitation for the TBL response

The stochastic pressure excitation due to turbulent boundary layer (TBL) flowing on the fuselage is an important contribution for the aircraft interior vibration and noise. The TBL can be modelled by using several models [18] but the predictive problem can become computationally challenging and needs trade-off between computational cost versus accuracy of the results [16,5]. In this work, a new method for the evaluation of the stochastic response is proposed, Pseudo Equivalent Deterministic Excitation ($PEDE_M$); it is based on the Pseudo Excitation Method, PEM [30], which is an exact representation using a modal decomposition of the cross-spectral density matrix of the load. In PEM, the extraction of the eigensolutions of

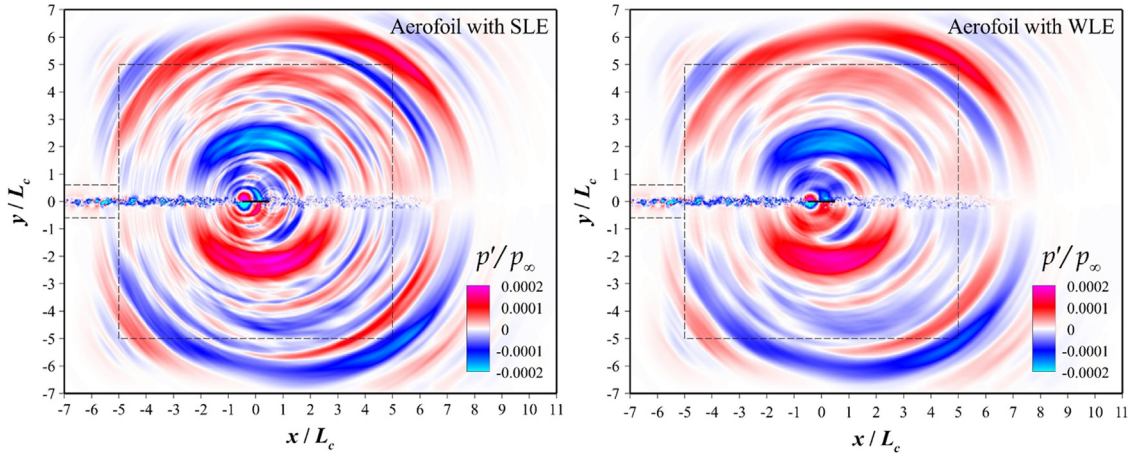


**Fig. 1.** A snapshot (sideview) of radiated aerofoil–turbulence interaction noise simulated with two different aerofoil geometries: SLE (left) and WLE (right) located in the middle of the domain (see [26] for details).

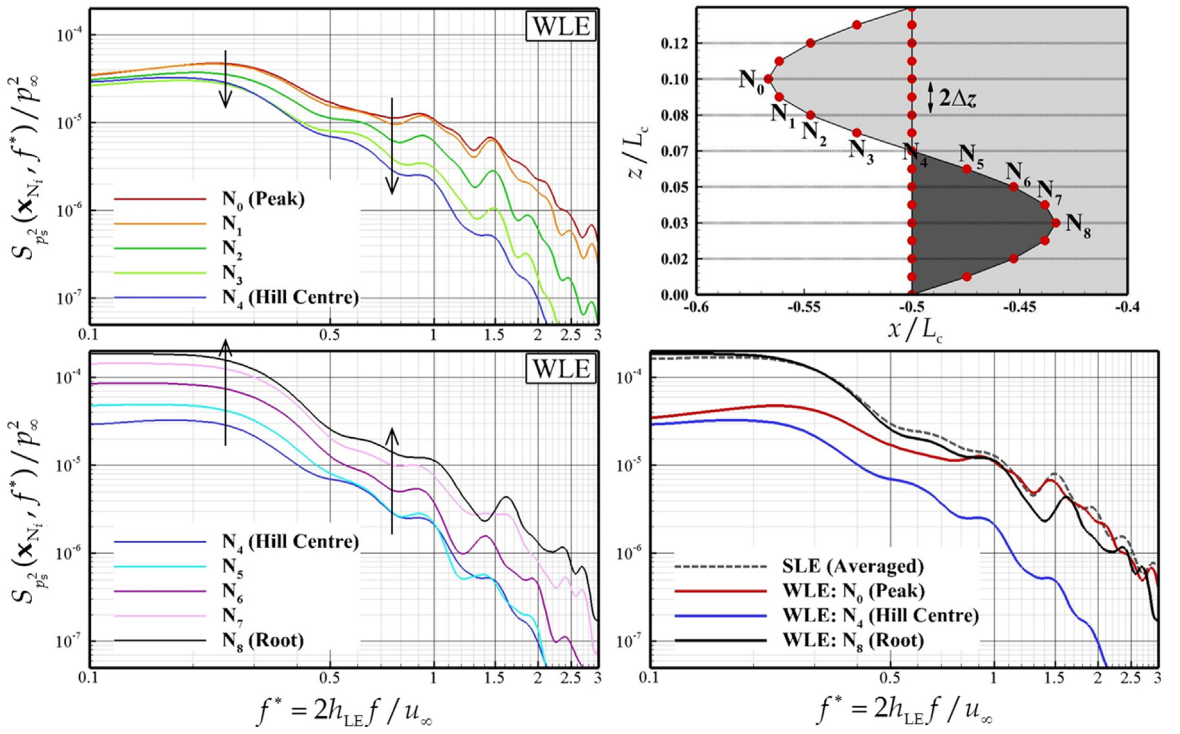


**Fig. 2.** Auto-spectra of surface pressure fluctuations along the WLE obtained at the probe points denoted in the figure, compared with the SLE case (see [27] for details).

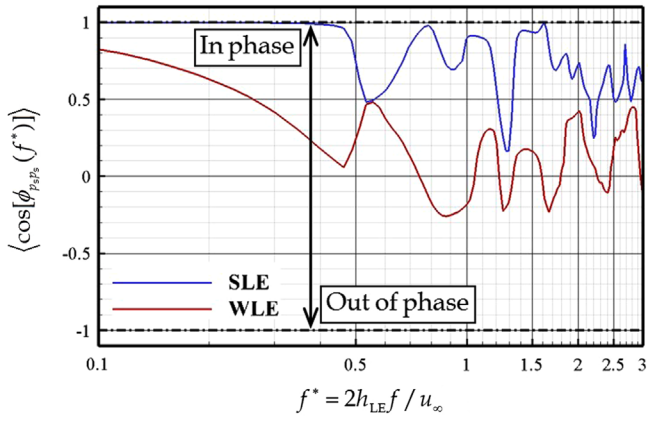


**Fig. 3.** Phase spectra averaged along the leading edge for comparison between the SLE and WLE cases (see [27] for details).

the load matrix is required at each frequency step: PEDE$_M$ tries to overcome this computational bottleneck by introducing some approximations. Three different approximations are proposed and thus modulated for the three frequency ranges accordingly with the characteristics of the load matrix.

A criterion to identify these frequency ranges is also proposed by introducing a dimensionless representation. The results show that the proposed approximations combine a good accuracy in representing the stochastic system response with a 40 percent of reduction of the computational costs if compared to a full stochastic response. The method is successfully applied to a simple 1D configuration which still presents the main features of a generic system. A more realistic test case is also presented consisting in a flexural plate and by invoking two approximations (low and high frequency ranges): even in this case the results are satisfactory (Fig. 4).

*Written by Sergio De Rosa* (*sergio.derosa@unina.it*), *Francesco Franco, University of Naples, Italy, Elena Ciappi, CNR-INSEAN, Italy.*

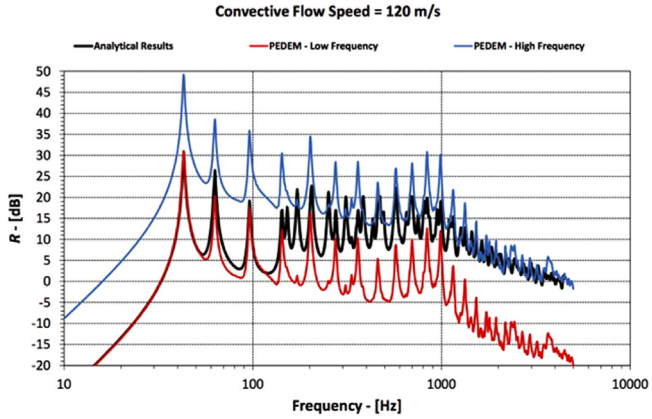


**Fig. 4.** Structural response: dimensionless metric ($R$) (dB) versus frequency (Hz): black, analytical solution; red, PEDE$_M$ low-frequency; blue, PEDE$_M$ high-frequency. (For interpretation of the references to color in this figure caption, the reader is referred to the web version of this paper.)

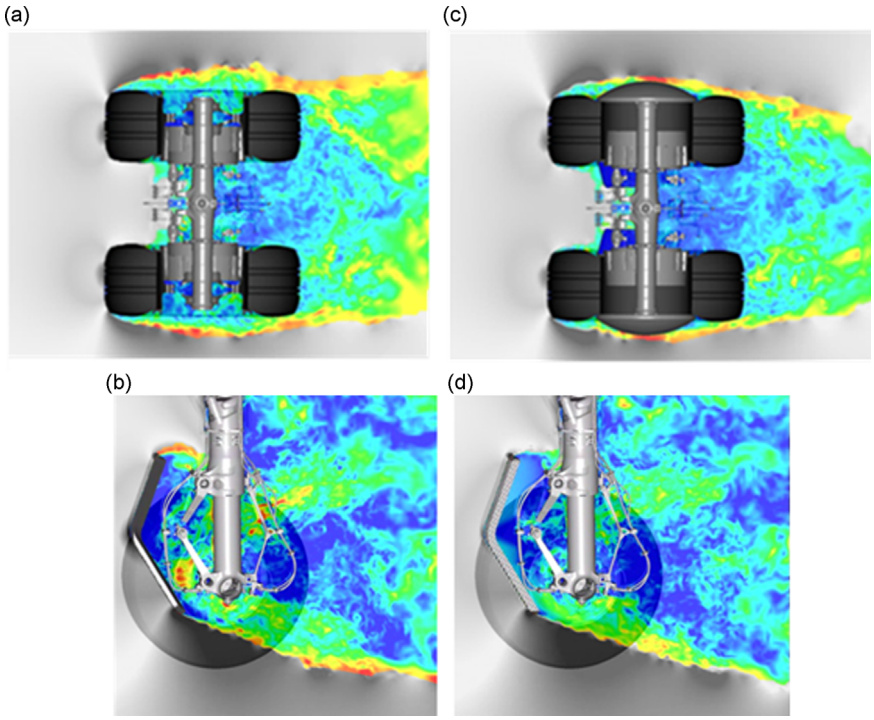


**Fig. 5.** (a) Instantaneous velocity maps for configuration without (top left) and with (top right) fairings. (b) Vertical cut between the wheels. Solid fairing surface (bottom left) and porous surface (bottom right).

### 3.3. *Detailed numerical approach for quieter landing gears*

In order to decrease the noise emission of the landing gear systems which is a significant part of the airframe noise during approach phase [11], Messier-Bugatti-Dowty has carried out numerical coupled LBM/CAA approach simulations with PowerFLOW on an in-service single-aisle two-wheel main landing gear [43]. The lower parts of the landing gear were modified with optimized fairings, leading to a calculated reduction of more than 2.5 EPNdB.

Three areas of the lower part of the gear were covered by optimized add-on fairings in order to reach a low noise configuration. The outer rims of the wheels are covered to decrease the interactions between the shear layer created on the front tyre and the cavity and to narrow the wake behind this part of the gear as shown in Fig. 5(a). Also, brake fairings shield the piston housing leading to noise reduction at middle and high frequency range. A third area covered by fairings is the torque link. The use of porous fairing reduces the velocity around the strut and makes it more homogeneous, as presented in Fig. 5(b), and thus acoustically more efficient [35].

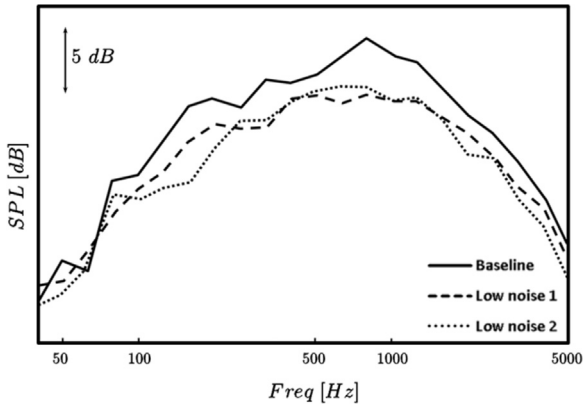


**Fig. 6.** Sound pressure levels of the baseline and low noise configurations at 90°, just underneath the landing gear.

The spectrum at 90° is presented in Fig. 6. The noise reductions reached with brake and rim fairings (low noise 1) impact the whole frequency range. The low noise 2 configuration slightly further improves the acoustic signature of the gear at low and higher frequency ranges.

*Written by Quentin Bouvy* (*quentin.bouvy@safranmbd.com*), *Safran Landing Systems, United Kingdom.*

## 4. Fan and jet noise

### *4.1. Installed aeroengine hybrid RANS-NLES of flow through an intake, fan, bypass duct and jet with wing, pylon and deployed flap*

The aerodynamics and noise produced by aeroengines is a critical topic in engine design. Hybrid Reynolds-Averaged Navier–Stokes-Numerical-Large-Eddy Simulation (RANS-NLES), has been used to investigate the influence of upstream internal geometry on jet flow and noise. Installed coaxial nozzles including an intake, wing and flap and internally, the fan, outlet guide vanes (OGVs) and other large features have been modelled. These large scale multi-fidelity, multi-physics calculations showed that inflow conditions only have a secondary effect on jet plume development and hence by inference noise. Upstream turbulence accelerates inner shear layer development, moving profiles of mean and fluctuating quantities slightly upstream [47].

Fig. 7 shows the setup and an instantaneous snapshot of the installed nozzle flow. The turbulence generated internally introduces a complex unsteady nozzle exit flow as shown in Fig. 8. Fig. 9 shows the time averaged axial and radial Reynolds stress contours showing turbulence transported downstream between the inner and outer shear layers.

*Written by James C. Tyacke* (*jct53@cam.ac.uk*), *University of Cambridge, United Kingdom and Mahak Mahak, Loughborough University, United Kingdom.*

### *4.2. Turbofan broadband noise predictions using a 3D ZDES rotor blade simulation*

Turbofan broadband noise prediction is a major concern for industry and probably the most challenging issue for Aeroacoustic community. The dominant source mechanism is attributed to the rotor turbulent wakes impacting the outlet guide vanes. Unsteady CFD computations of the full rotor–stator stage are generally out of reach so that interaction noise is commonly assessed using analytical models (related to Amiet theory) and averaged turbulence characteristics issued from a steady RANS calculation and isotropic homogeneous turbulence assumption. A hybrid RANS-LES computation of a single rotor blade has been investigated at ONERA [38] to provide a full description of the turbulent wakes directly entered as input to an Amiet-based code [39]. Simulations are performed using the ONERA solver *elsA* and adopting a Zonal Detached Eddy Simulation (ZDES) approach initially developed by Deck [10]. It permits to impose a continuous transition between RANS and LES, but with a more flexible choice adapted to the nature of the local flow. The reliability of this approach is checked thanks to the comparisons of turbulent velocity and acoustic spectra respectively with hot-film probe and microphone measurements performed in Snecma engine test rig. A quite good agreement is shown between numerical and experimental turbulent velocity spectra and also von Kármán spectrum model (Fig. 10), when mean turbulence characteristics are well adjusted. Moreover, sound pressure and power spectra in the outlet duct predicted by ZDES-Amiet coupling are reasonably close from the available measurements, and not so far from RANS-based ones addressed too (Fig. 11).

*Written by V. Bonneau, C. Polacsek* (*cyril.polacsek@onera.fr*), *L. Castillon, J. Marty, Onera, Châtillon, France and M. Gruber, Snecma Villaroche, France.*

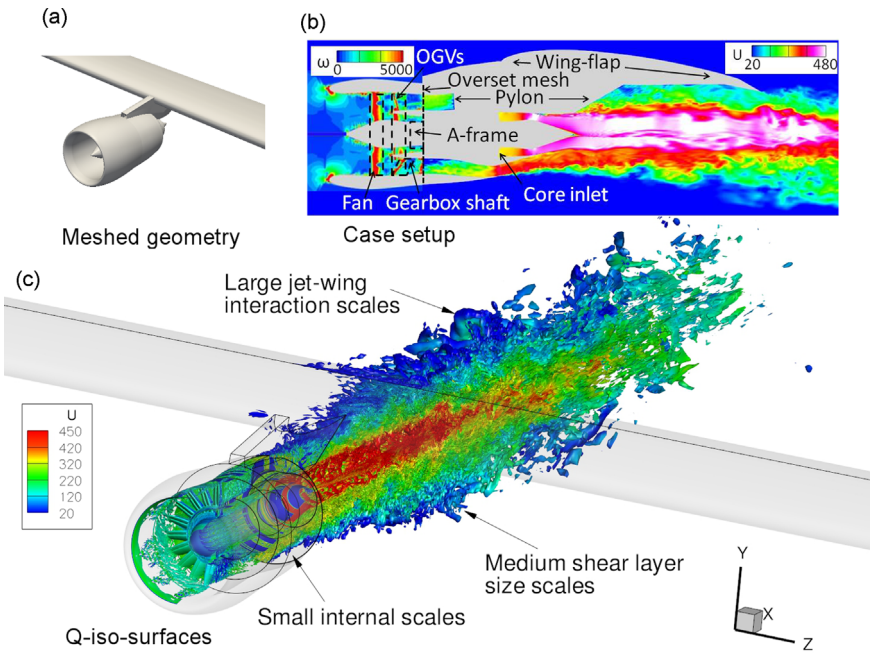


**Fig. 7.** Instantaneous snapshot showing (a), geometry that is meshed, (b), the case setup and (c), Q-criterion iso-surfaces highlighting the range of turbulent scales that are resolved.

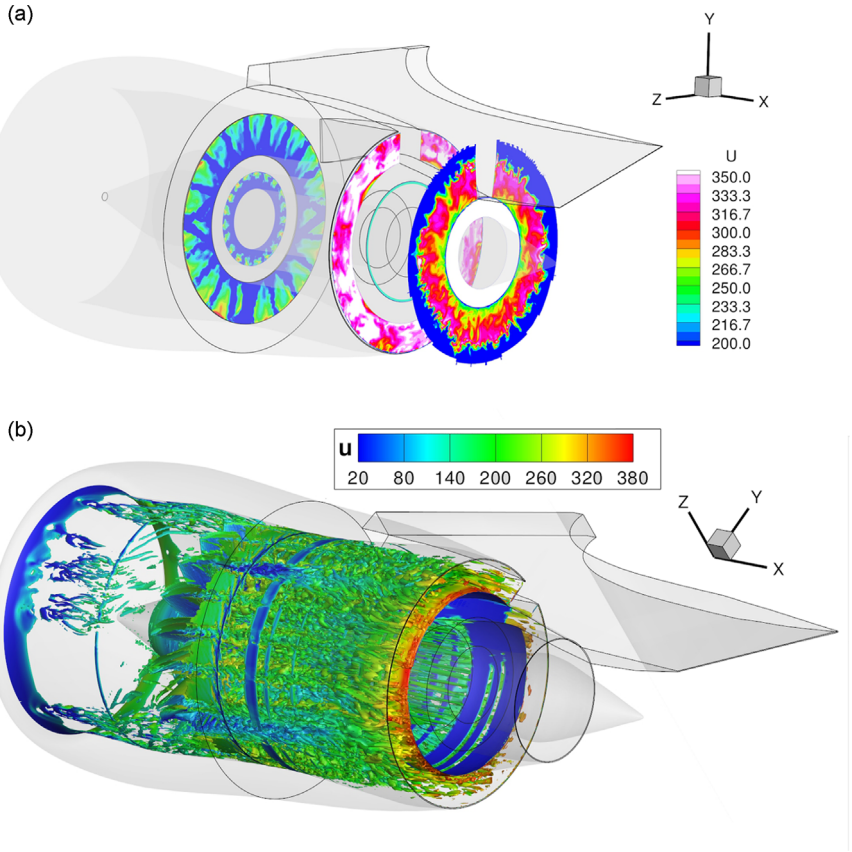


**Fig. 8.** (a) Complex upstream axial flow field at different axial planes. (b) Q-isosurfaces showing internal turbulence.

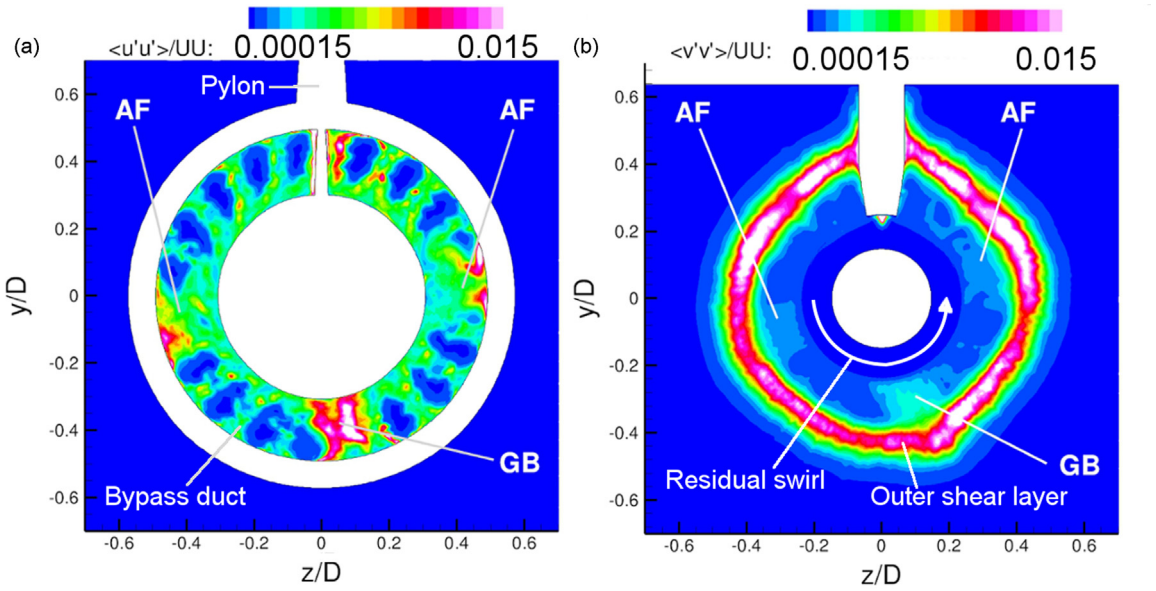


**Fig. 9.** Reynolds stress contours (a), axial stress upstream of the nozzle exit, (b), radial stress downstream of the nozzle exit. GB and AF indicate the upstream gearbox shaft and A-frames respectively.

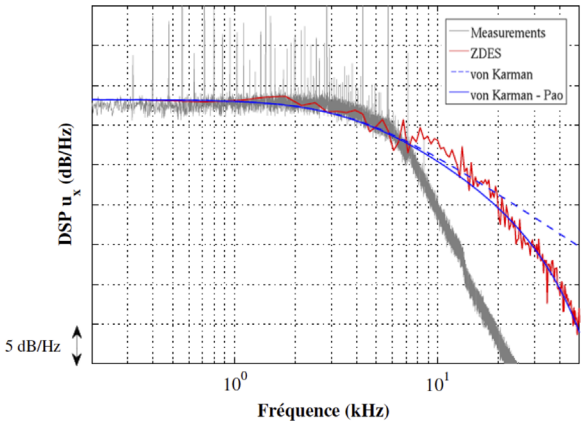


**Fig. 10.** PSD of axial turbulent velocity at 57% span.

## 5. Aircraft interior noise

### 5.1. *Fuselage excitation during cruise flight conditions: CFD based prediction of pressure point spectra*

In the last fifty years many semi-empirical models to predict surface pressure fluctuations beneath turbulent boundary layers (TBL) have been developed for a large variety of test conditions. Nowadays, the relevance of the TBL as a source of cabin interior noise is steadily increasing, due to quieter aircraft engines. Therefore DLR and Airbus jointly investigated that the accuracy of various publicly available semi-empirical pressure point spectra models has been investigated on various regions of DLR's Airbus A320, ATRA [28]. A large validation database was used, involving in-flight measurements at different flight levels and Mach numbers [44]. Overall, it is shown that today's models provide a large scatter among the predicted spectra (Fig. 12). Even the most suitable approaches are not generally applicable to all relevant positions at the fuselage. Particularly in regions with high turbulence kinetic energy (TKE), measured auto-spectra cannot be reproduced with sufficient accuracy. The TKE was identified as one of the main parameters (Fig. 13), influencing auto-spectra on a fuselage. By using this quantity to scale auto-spectra, outer scaling and peak region were brought to a perfect collapse (Fig. 14). The original GOODY model [17] cannot predict measurements sufficiently (Fig. 15). This indicates the need for more universally applicable computational fluid dynamics (CFD)-based surface pressure prediction methods. Therefore, a new model, based on the modelling approach of GOODY [17], was developed. The CFD data is calculated with DLR's TAU code, using a Reynolds

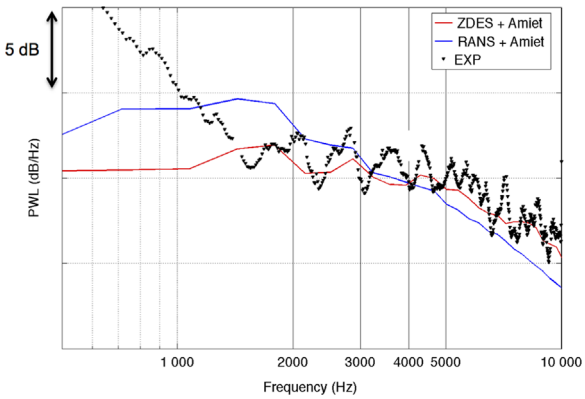


**Fig. 11.** PWL spectra in the bypass duct issued from calculations and experiment.

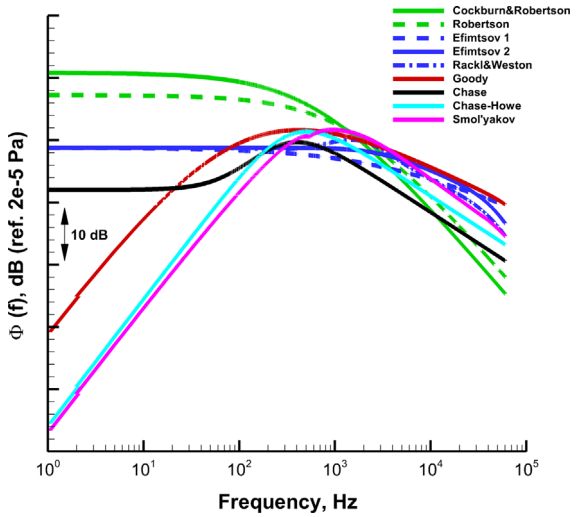


**Fig. 12.** Comparison of predictions from publicly available auto-spectra models; $Ma=0.78$, FL 350, $x=12.5$ m.

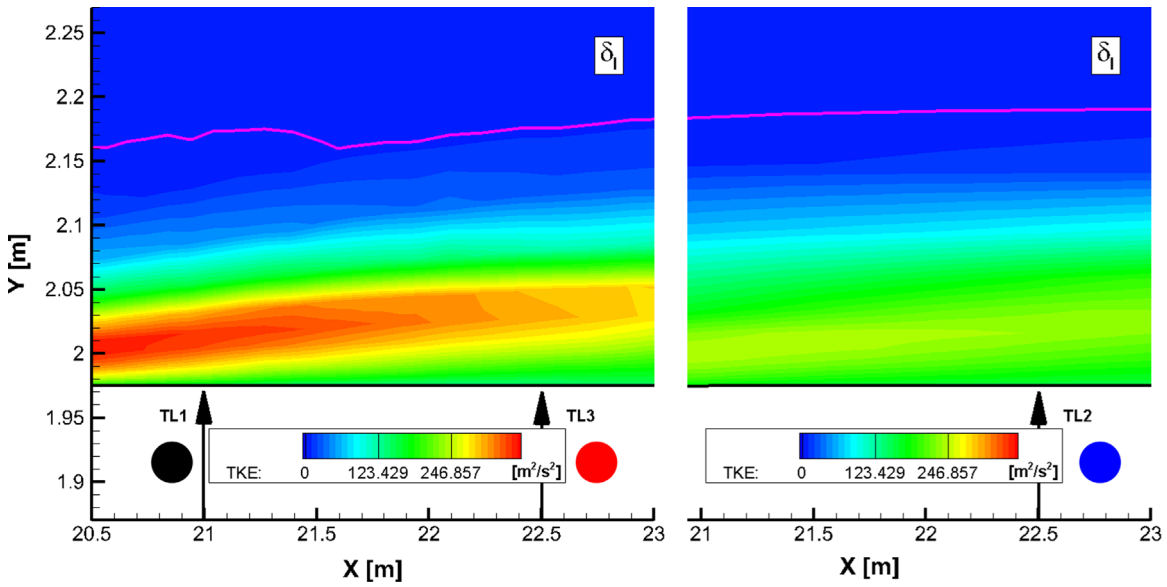


**Fig. 13.** TKE distribution and local boundary layer thickness (TAU calculation) in a vertical slice above analyzed sensors.

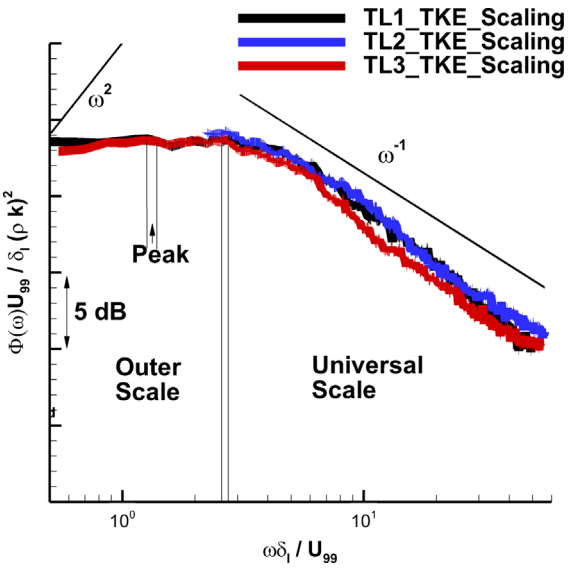


**Fig. 14.** Measured spectra, scaled by TKE maximum value.

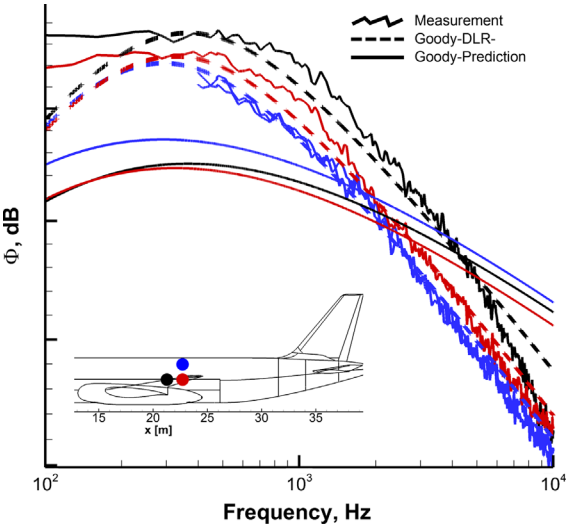


**Fig. 15.** Comparison of measurement data with original GOODY and DLR modified GOODY prediction that takes the turbulence kinetic energy from CFD into account. Measurement locations are depicted on the aircraft sketch.

stress (RSMg) turbulence model. Finally, a satisfying prediction of the measured spectra can be ensured (Fig. 15) by the new model.

*Written by Alexander Klabes* (*alexander.klabes@dlr.de*), *Christina Appel, Michaela Herr, German Aerospace Center* (*DLR*), *Lilienthalplatz 7, D-38108 Braunschweig, Germany, Sören Callsen, Airbus Operations GmbH, D-21129 Hamburg, Germany.*

### 5.2. *Numerical investigation for wall pressure fluctuations using synthetic turbulence*

Wall pressure fluctuations beneath a flat plate turbulent boundary layer (TBL) were computed from a Poisson equation with synthetic turbulence, see [22]. The Poisson equation was solved utilizing a fast Fourier transform with Hockney's method [21]. Due to its efficiency, the applied procedure enables the study of the fluctuating pressure field at high Reynolds number. The procedure aims to resolve only the largest eddies in the TBL, since the smaller neglected scales that are responsible for the high frequencies and for most practical applications of flow-induced structural vibration have no relevance due to their poor transmission efficiency.

The source terms on the right-hand side of the Poisson equation were provided by the Fast Random Particle-Mesh Method [14]. Both, mean-shear (ms) turbulence interaction and turbulence–turbulence (tt) interaction were calculated. Fig. 16(a) shows the spectral dominance of the ms-term over the whole frequency range. A very good agreement is found

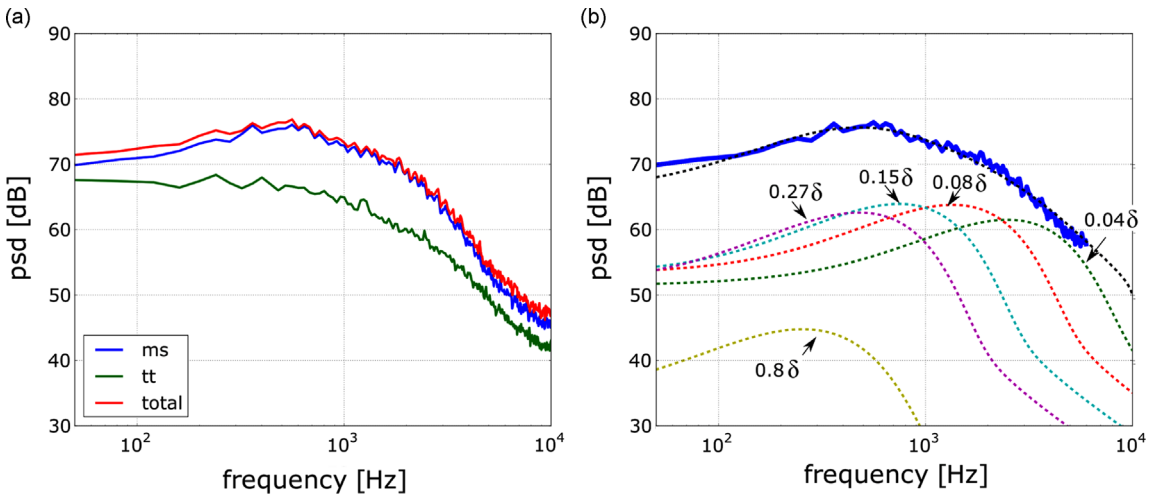


**Fig. 16.** Wall pressure fluctuations: (a) spectra of $p_{ms}$, $p_{tt}$ and $p_{total}$, (b) spectra of $p_{ms}$ and the contribution from different wall-normal positions; (-), simulation result with Corcos correction; (- -), theoretical predictions using the mean flow one-point statistics and the two-point cross-correlation model.

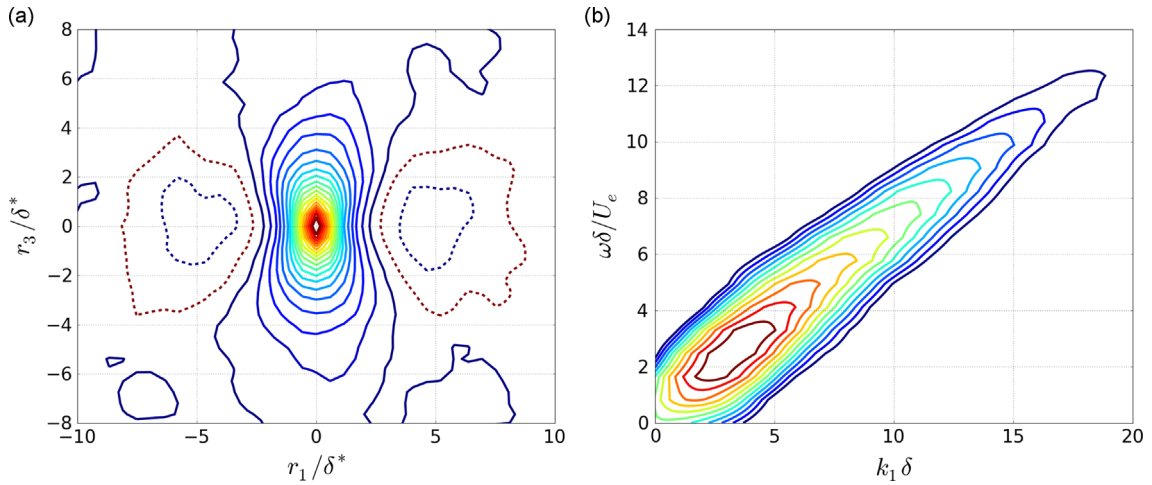


**Fig. 17.** (a) Contour plot of spatial correlations; (-), iso-contours, 0–0.9 with increment of 0.05; (- -), iso-contours, −0.05 and −0.1, (b) contour plot of wavenumber–frequency spectra $\Phi_{pp}(k_1,\omega)$; iso-contours, −59 dB to −49 dB with increment of 1 dB.

between theoretical and simulated spectrum including a Corcos correction [6] for finite pressure tap diameter, Fig. 16(b). The theoretical contribution to the wall pressure fluctuations from different wall-normal positions is highlighted in Fig. 16(b). Good agreement for correlation characteristics is found between the simulations and results from other investigators. The spatial correlation plot illustrates an elongated shape of iso-correlations in the transverse direction and a negative correlation region in the longitudinal direction, see Fig. 17(a). Wavenumber–frequency spectra were calculated showing a well-defined convective ridge, Fig. 17(b).

*Written by Nan Hu* (*nan.hu@dlr.de*), *Nils Reiche and Roland Ewert, DLR, Germany.*

## 6. Techniques and methods in aeroacoustics

### *6.1. Direct aeroacoustic simulation of acoustic feedback phenomena on a side-view mirror*

The generation of tonal noise at a realistic side-view mirror is investigated by large eddy simulation and direct noise computation based on the compressible Navier–Stokes equations. The underlying mechanism resembles the aeroacoustic feedback loop leading to narrow-band noise emission from airfoils at low Reynolds number [1,25]. We employ the high order discontinuous Galerkin spectral element method [20] to ensure accurate representation of the instabilities in the transitional boundary layer and the propagation of sound.

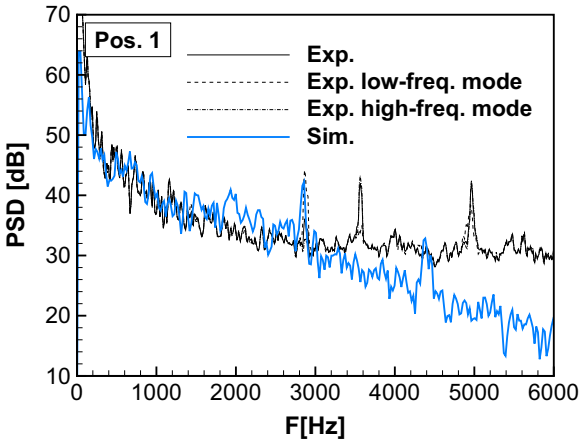


**Fig. 18.** Power spectral density at the microphone position for simulation and experiment. Due to an intermittent alternation between two different tones in the experiment, we plot two additional spectra obtained through conditional averaging.

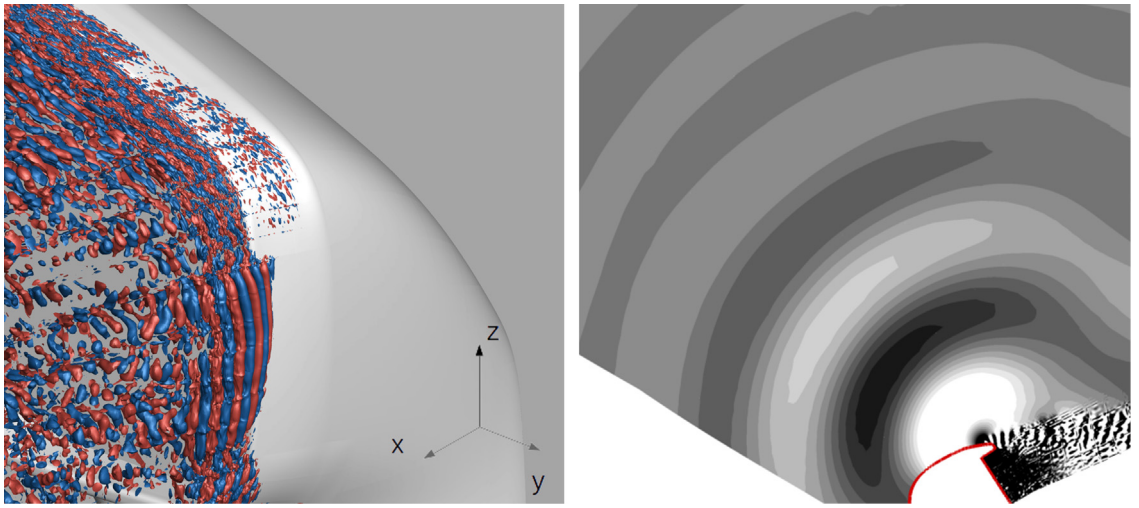


**Fig. 19.** Structure of the Fourier mode at 2827 Hz. Left: coherent structures at the trailing edge visualized by means of isosurfaces of the velocity fluctuation in streamwise direction, right: pressure fluctuation contours in a $z = \text{const.}$ plane.

Our simulation predicts tones emitted from the same regions as in corresponding experiments, one of them close to one of the experimental tone frequencies (see Fig. 18). These tones originate through the interaction of coherent vortices with the trailing edge in a region downstream of laminar separation, visualized by isosurfaces of velocity fluctuations in Fig. 19 (left) and contours of fluctuation pressure (right).

A global perturbation analysis reveals a global instability: a self-sustaining feedback loop comprising convective growth in the separated shear layer, scattering at the trailing edge, upstream radiation and natural receptivity at a rounded kink in the shape of the mirror (see Fig. 20). The Ritz spectrum of a dynamic mode decomposition (DMD) of the perturbation simulation plotted in Fig. 21 shows that modes with discrete frequencies are selected by the mechanism, where the dominant ones coincide with the tonal components of the developed flow. It is shown that the observed tonal modes satisfy the phase condition associated with the feedback loop [37].

Tonal noise generation through aeroacoustic feedback has been simulated here for the first time for a complex geometry and demonstrates the importance of feedback effects from the acoustic to the hydrodynamic field which are neglected in many cases.

*Written by Hannes M. Frank (frank@iag.uni-stuttgart.de) and Claus-Dieter Munz (munz@iag.uni-stuttgart.de), Institute for Aerodynamics and Gas dynamics, University of Stuttgart, Germany.*

### *6.2. Decorrelation of acoustic wave propagation through the shear layer in open jet wind tunnel*

The impact of decorrelation of acoustic waves when passing through the shear layer in open jet wind tunnels is usually neglected. The decorrelation however results in both a loss of image resolution and a corruption of sound levels in the

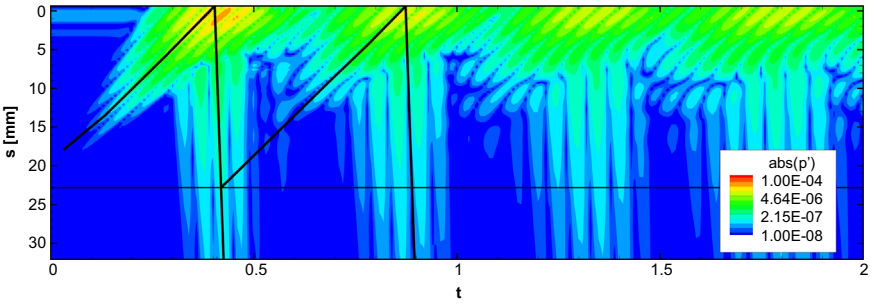


**Fig. 20.** Temporal evolution of the perturbation wall pressure, $s$ denotes the distance to the trailing edge. Downstream and upstream running components indicate the alternation between amplified convective instabilities and upstream running acoustic wave packets.

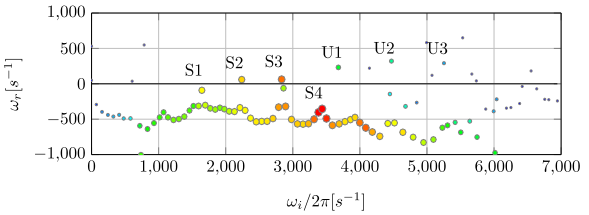


**Fig. 21.** Ritz value spectrum from DMD of the perturbation simulation. Discrete feedback modes originating from the side and the upper surface are labeled S1–S4 and U1–U3. Notice the coincidence of S3 to the main tonal frequency.

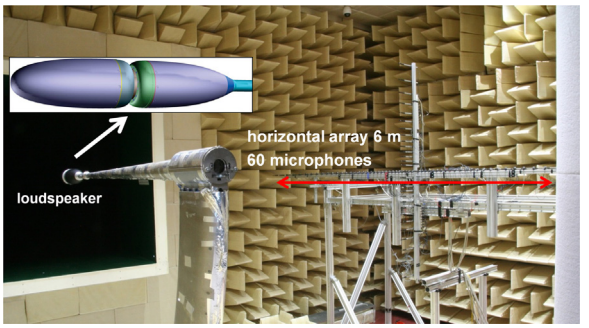


**Fig. 22.** Horizontal microphone array and aerodynamically covered loudspeaker in the DNW-NWB open test section.

beamforming result. For achieving accurate source levels from aeroacoustic measurements and designing suitable array geometries, an analytical prediction of the decorrelation is needed. The coherence function of waves propagating through random media has been widely studied in the field of astrophysics. Pires et al. [36] utilized this approach and compared the theoretical coherence function to measured data from a closed test section. Using a Markov approximation a parabolic wave-equation was derived in order to model isentropic turbulence perpendicular to the direction of wave propagation. This theoretical model was now compared to a DLR measurement in the open-jet DNW-NWB wind tunnel [13]. A 6 m linear array was placed outside the flow. Inside the flow an aerodynamically covered loudspeaker was placed and driven by white noise (Fig. 22). At low frequencies below 10 kHz the decorrelation is mostly caused by the background noise in the wind tunnel. Therefore, the measured data is compensated by a background noise subtraction (Fig. 23). Using background subtraction, the Markov model is capable of predicting the coherence loss due to the turbulent shear layer (Fig. 24).

*Written by Daniel Ernst* (*daniel.ernst@dlr.de*), *Carsten Spehr and Tobias Berkefeldt, DLR, Germany.*

### *6.3. CAA computation of interaction between single stream jet and NACA0012*

A generic jet installation noise problem was studied in the framework of the EU project JERONIMO using a single stream jet at $Ma_j$=0.6 with ambient conditions at rest in combination with a rectangular unswept wing. The wing sections are defined by a NACA0012 airfoil and the airfoil chord is oriented parallel to the jet axis. The chord length is four nozzle diameters. The wing trailing edge (TE) is located one nozzle diameter vertically above the jet axis $H/D_j = 1$ and has axial displacement $L/D_j = 4$ from the nozzle exit plane center.

The present CAA computation [14] provides a partly scale resolving simulation using nonlinear disturbance equations (NLDE) in conjunction with active forcing from a stochastic method (FRPM) for turbulent backscattering. Quantitative levels

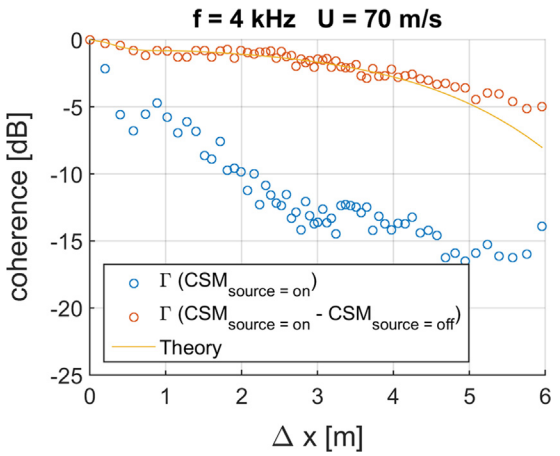


**Fig. 23.** Coherence loss over microphone spacing, with (red) and without (blue) background noise subtraction. (For interpretation of the references to color in this figure caption, the reader is referred to the web version of this paper.)

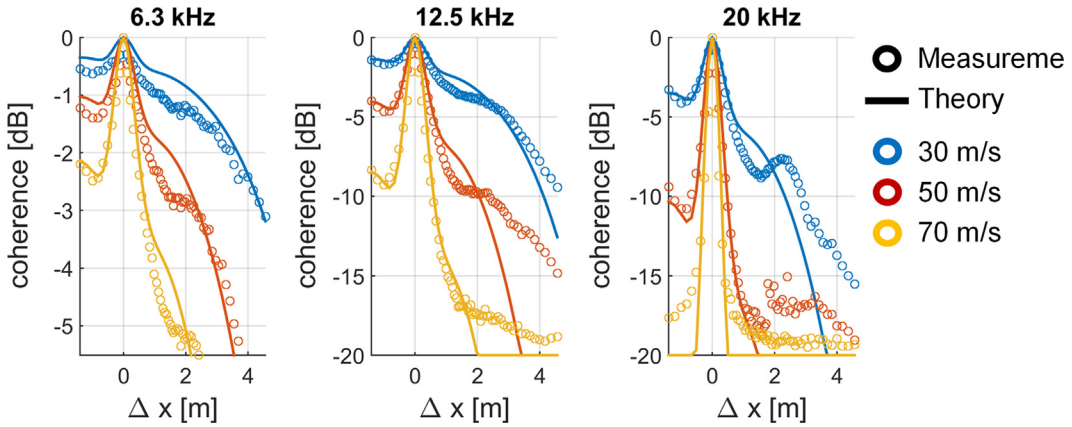


**Fig. 24.** Comparison of prediction and measured coherence loss over microphone spacing at third octave bands (6.3 kHz, 12.5 kHz, 20 kHz) and different flow speeds (30 m/s, 50 m/s, 70 m/s).

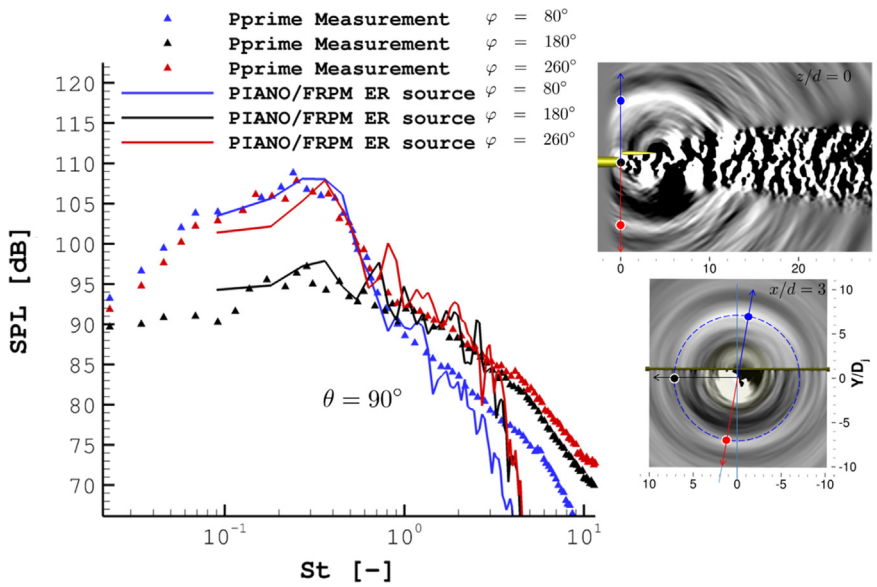


**Fig. 25.** Sound pressure level spectra of CAA computation and measurement for a configuration with Pprime single stream nozzle ($Ma_j = 0.6$, $Ma_\infty = 0.0$) and NACA0012 in constellation ($H/D_j = 1$, $L/D_j = 4$) at $\theta = 90^\circ$.

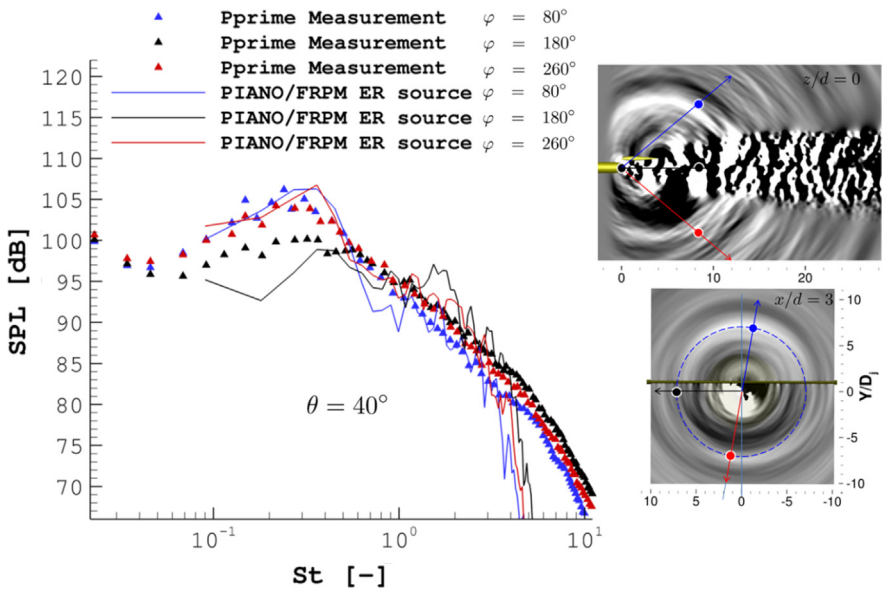


**Fig. 26.** Sound pressure level spectra of CAA computation and measurement for a configuration with Pprime single stream nozzle ($Ma_j = 0.6$, $Ma_\infty = 0.0$) and NACA0012 in constellation ($H/D_j = 1$, $L/D_j = 4$) at $\theta = 40^\circ$.

of the backscattering are derived from the eddy relaxation source model proposed by Ewert et al. [15]. The numerical approach has been also verified using an isolated nozzle with $Ma_j$=0.9 as described by Neifeld et al. [34].

Interaction noise spectra are shown in Fig. 25 in comparison with measurements [4]. The low frequency hump in the spectrum can be attributed to trailing edge noise caused by the scattering of hydrodynamic instabilities in the jet. The good match between measured and computed spectra for different azimuthal and polar angles leads to the conclusion that effects like shielding and relative levels of jet and TE noise are numerically well reproduced.

*Written by Andrej Neifeld* (*andrej.neifeld@dlr.de*), *Christina Appel, Jürgen Dierke, Roland Ewert, Jan W. Delfs, DLR, Germany.*

### *6.4. Novel noise-source-identification technique combining acoustic modal analysis and a coherence-based noise-source-identification method*

A novel technique is presented [8,9], which combines the fields of coherence-based noise-source identification with acoustic modal analysis. Coherence-based noise-source-identification techniques apply the coherence function, estimated between pairs of dynamic pressure sensors, to identify the relative contributions of one or several noise sources to the total noise measured at a location of interest. Acoustic-modal-analysis techniques use arrays of microphones to decompose the pressure field at an axial location of a duct into constituent modal amplitudes (Fig. 26). Conditional Spectral Analysis: Modal is the primary novel technique presented herein, and uses conditional spectral analysis developed in earlier work [7,2] to allow the beneficial capabilities of each of these well-regarded fields to be combined into one method. The technique allows the total modal pressure field measured in a duct to be decomposed into parts associated with contributing uncorrelated noise sources. The techniques efficacy is validated with a two noise-source-region experimental rig, e.g. Fig. 27. The modal-conditional-spectral-analysis technique represents a significant advancement in noise-source identification, and may be applied to a full-scale aeroengine to identify the specific contributions of core-noise sources within the engine to the amplitudes of the acoustic modes propagating through the engine exhaust, e.g. Fig. 28. This added acoustic modal information can be used to predict the relative contribution of these noise sources to the total noise radiated from the engine and into the far field. Knowledge of the contributions of each core-noise-source contribution to the modal content propagating through the engine exhaust also allows for better mitigation through optimized liner designs and location.

*Written by Gareth J. Bennett* (*gareth.bennett@tcd.ie*), *School of Engineering, Trinity College Dublin, Ireland, Ian Davis, Bell Labs, Ireland.*

### *6.5. Acoustic source identification on VEGA launch pad at lift-off*

During VV05 of VEGA launcher in Kourou, microphone array measurement was performed by D'Appolonia. The circular array (2 m in diameter) composed of 32 microphones regularly spaced was installed on a lightning pylon, approximately at the payload fairing level, and oriented toward the exhaust duct. ONERA was in charge of the acoustic post-treatment in order to identify the acoustic sources on the launch pad during lift-off. Measurements and post-processing were done for VITROCISET, under the supervision of ESA.

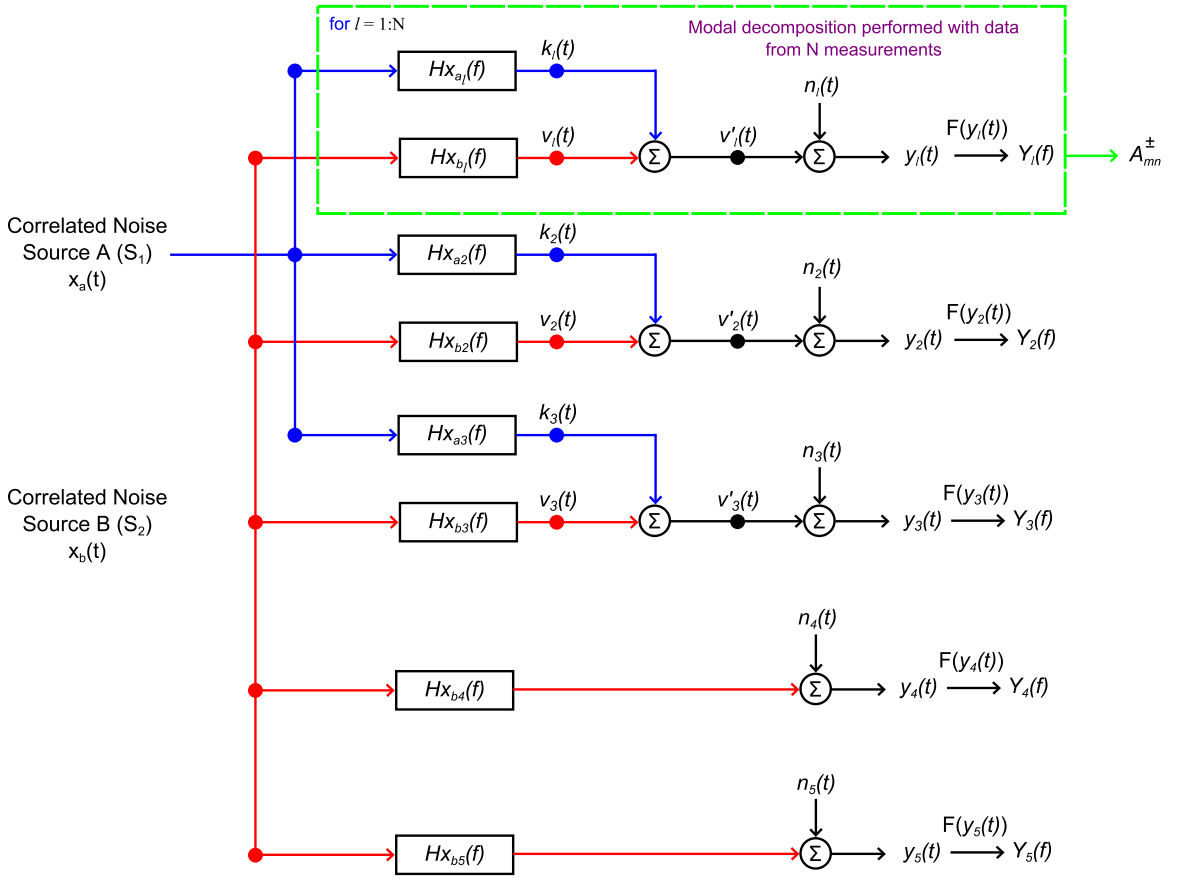


**Fig. 27.** CSA: modal five-output-technique model for the scenario shown in Fig. 28; measurement $Y_1(f)$ has been replaced by $A_{mn}^{\pm}$, the complex modal amplitude of the $(m, n)$ mode.

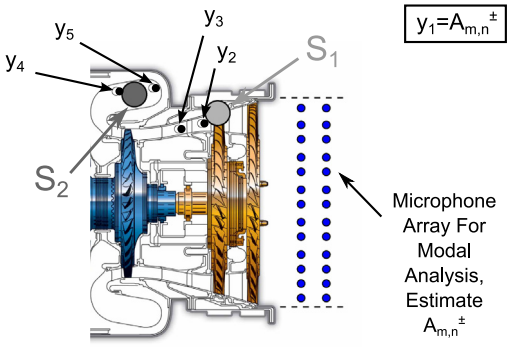


**Fig. 28.** Simplified representation of acoustics inside a turboshaft engine duct; in this experimental setup, a circumferential array has been installed in the exhaust duct.

After specific preliminary steps to obtain the Cross-Spectral Density Matrices in the context of inherent short and non-stationary acoustic data, two identification methods were applied: classical beamforming [24] and deconvolution process (DMS) based on DAMAS method [3]. Three source scanning plans were defined (Fig. 29): two horizontal ones (at the level of the jet deflector and on the table) and a vertical one including the launcher.

Results obtained with DMS are shown in Fig. 30, just after the beginning of lift-off. Two main sources are highlighted: (i) from the launch table, attributed to openings from which the noise produced below the table comes out or to impact of jet flow onto the table; (ii) from the duct attributed to noise produced below the launch table that comes out by the duct, including possible reflection on the sloping part of the duct floor.

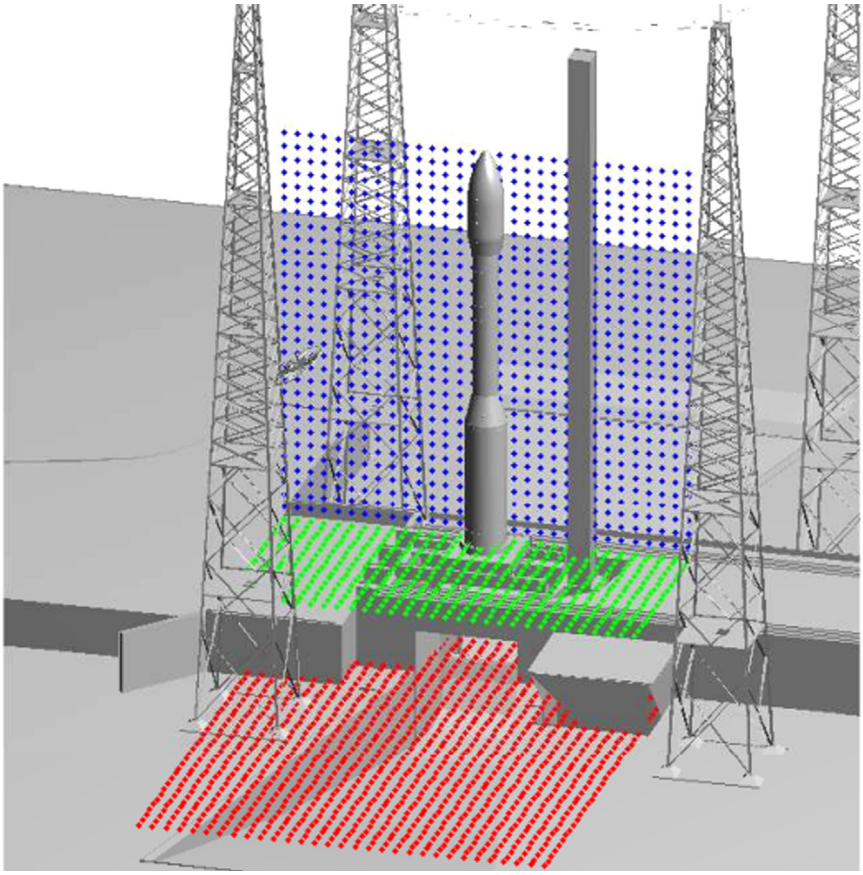

**Fig. 29.** VEGA launch pad and source scanning plans.

The overall results provided the evolution with time of acoustic sources on VEGA launch pad for all frequencies of interest, giving guidelines to improve the acoustic environment during lift-off.

*Written by Jean Bulté* (*jean.bulte@onera.fr*), *ONERA, France.*

### 6.6. Numerical characterization of noise sources by a simplified landing gear using advanced simulation and analysis techniques

In its effort towards the mitigation of aircraft noise, over the past decade, ONERA developed an advanced hybrid approach [40] that relies on the weak-coupling of unsteady Computational Fluid Dynamics (CFD) and Computational AeroAcoustics (CAA) methods/solvers. After it was validated through academic test cases of increasing complexity, such advanced hybrid approach was successfully applied to various realistic problems of aircraft noise [42,40], such as the aeroacoustics of an in-flight simplified nose landing gear [41] (LAGooN program [32], supported by Airbus). Lately, and based on the CFD-CAA simulations outputs acquired over the LAGooN configuration, the latter's noise sources were further characterized through the use of advanced signal processing techniques; once acquired over virtual microphone arrays matching those used in the experiments, the CFD-CAA signals were processed following two distinct array methods of source localization, namely Classical Beam Forming (CBF) and Deconvolution Approach For Maps of Acoustic Sources (DAMAS). The localization results obtained (see right side of Fig. 31) were found to be coherent with the ones that had been originally derived on the basis of the experimental signals [32], as well as with the conclusions that had been made about the NLG noise physics. In the wake of such noise source characterization exercise, a benchmark test case shall now be disseminated through the NASA-supported Array Analysis Methods workshop, so as to help the community benchmarking the diverse signal processing techniques commonly employed for localizing aircraft noise sources.

*Written by Stéphane Redonnet* (*stephane.redonnet@onera.fr*) *and Jean Bulté, Onera, France.*

### 6.7. Extended version: improving the DAMAS2 results for wavenumber-space beamforming

When performing beamforming, the result will be affected by array properties like the transducer distribution. This can be shown using a synthetic source distribution (Fig. 32(a)) which is convolved with the array properties (Point Spread

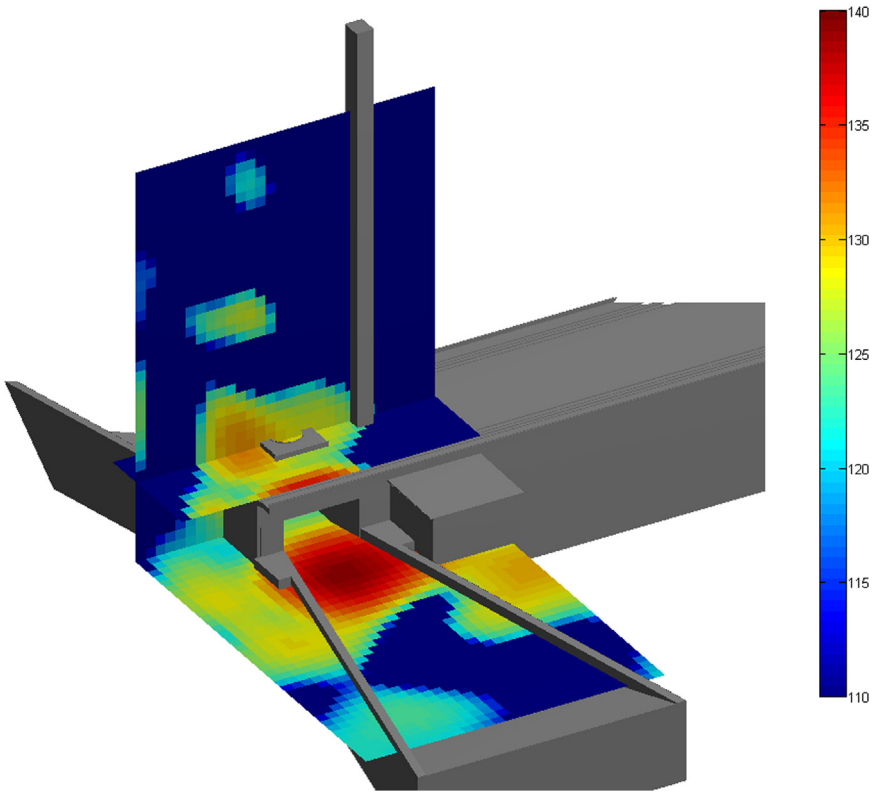


**Fig. 30.** Acoustic maps at 500 Hz (launcher removed) altitude between 5 and 10 m.

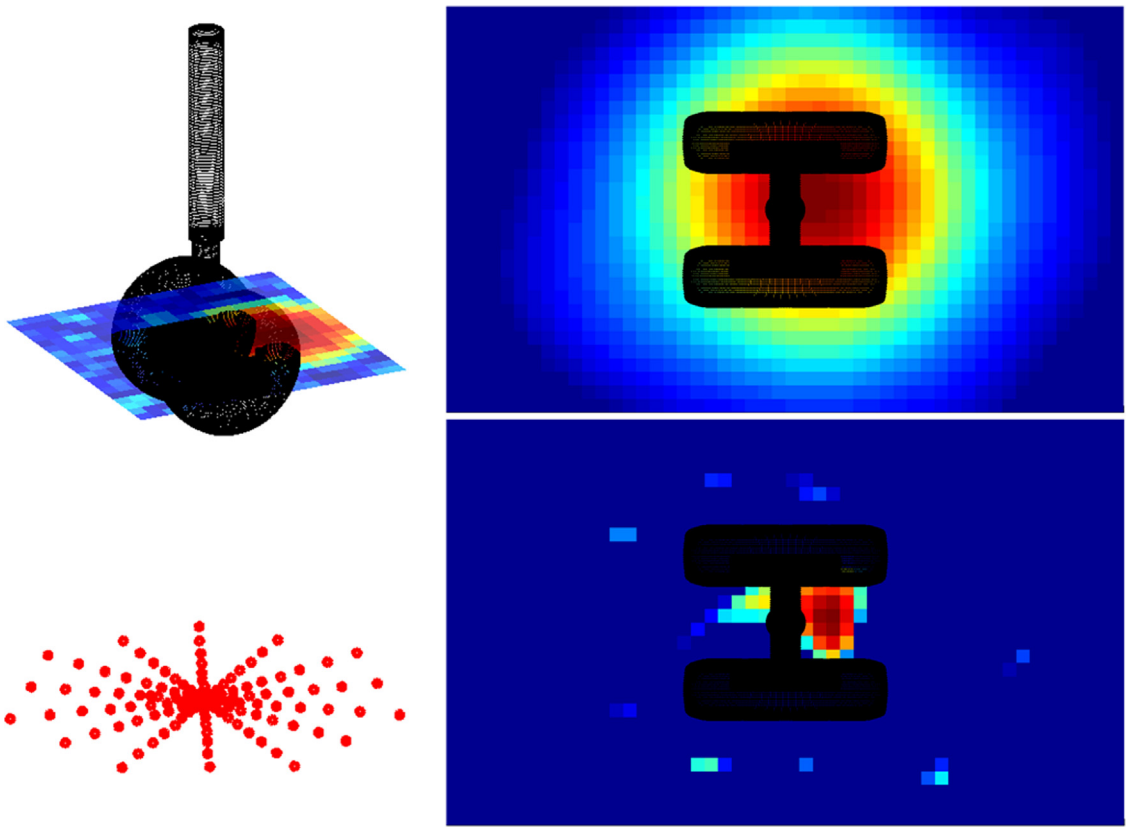

**Fig. 31.** Numerical characterization of the noise sources by an in-flight simplified landing gear (LAGooN program) using CFD-CAA weakly coupled calculations and array-based signal processing techniques. Left: mid-field antenna of virtual array microphones.

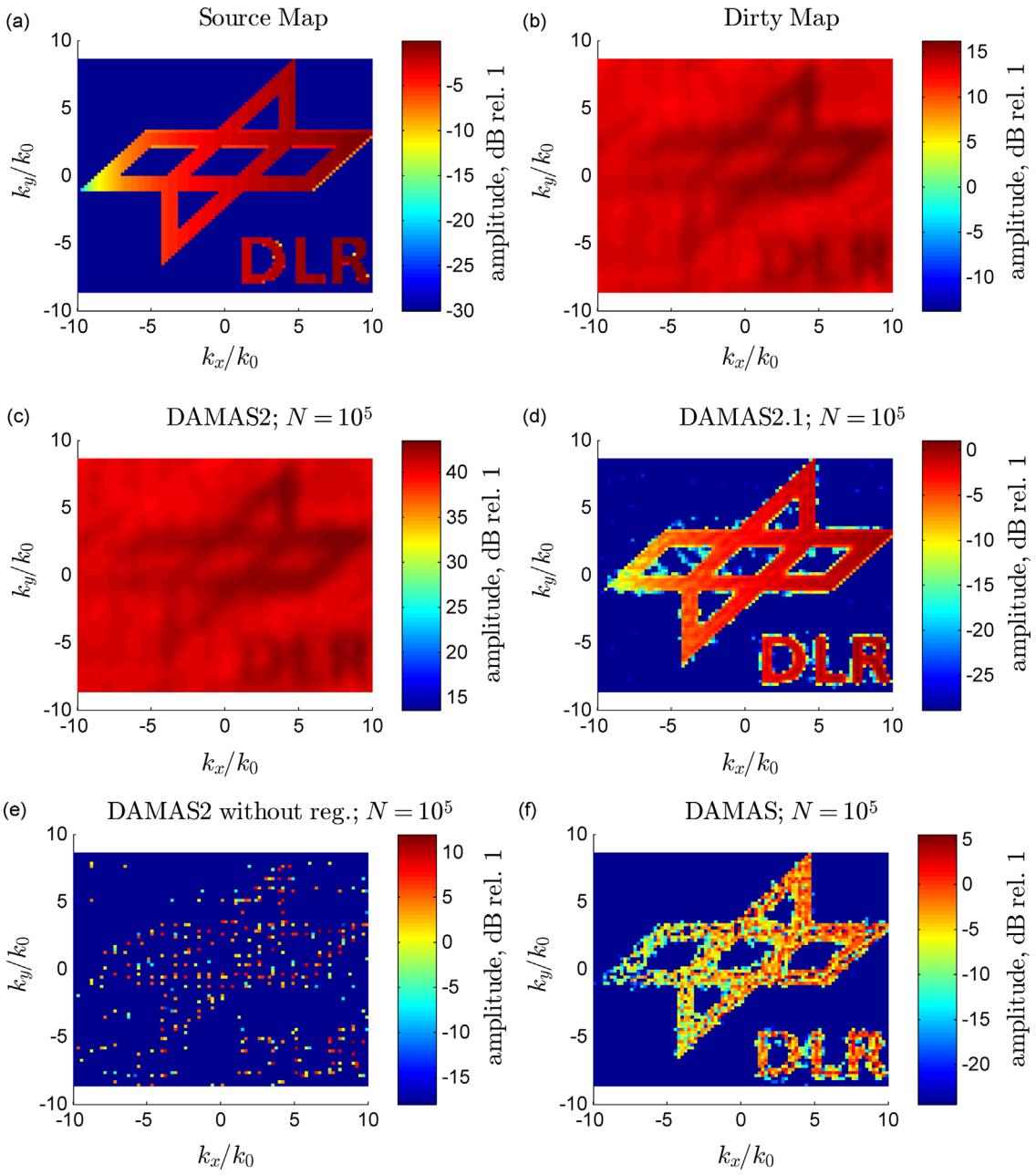


**Fig. 32.** Comparison of DAMAS-type deconvolution algorithms applied to a synthetic case at 1000 Hz after $10^5$ iterations.

Function or "PSF") – and results in the dirty map (Fig. 32(b)). In the present case, the maximum amplitude detected is significantly higher than the maximum amplitude of the source and the contrast of the map is reduced. In order to re-obtain the source maps from the measured data, deconvolution procedures are applied. The DAMAS2 algorithm [12] is a computationally efficient algorithm which can be applied to special cases, where the effect of the array does not depend on absolute transducer position, but only on relative positions (shift invariance).

It was found that the reconstruction process within the algorithm can be improved by extending the space over which the PSF is calculated. Four versions of the DAMAS-family – the original DAMAS [3], DAMAS2 with and without regularization filter, and the here proposed derivative DAMAS2.1 – are all applied the same set of synthetic data and their results are compared [19].

DAMAS2.1 improves the results compared to the DAMAS2 algorithm (residual shown in Fig. 33) as the new variation avoids the step which necessitates the regularization filter. It converges faster than the DAMAS algorithm for – as DAMAS2 –

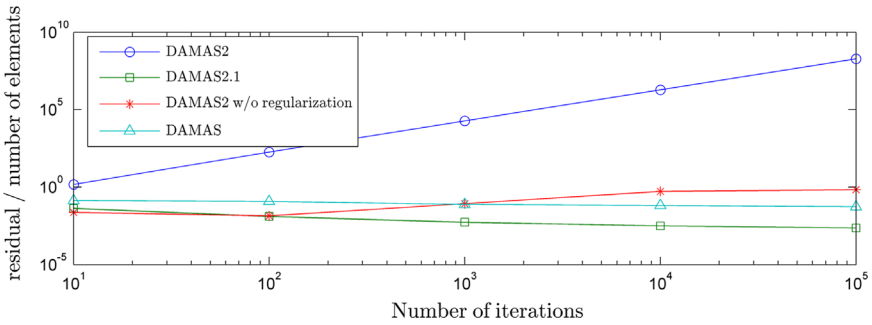


**Fig. 33.** Normalized residual at 1000 Hz: DAMAS2.1 and DAMAS converge; DAMAS2 without regularization finds an intermediate solution; DAMAS2 diverges due to the limitations applied by the regularization filter.

it uses a Richardson iteration rather than a Gauss–Seidel method. The computational effort of DAMAS2.1 is comparable to DAMAS2 and reduced by a factor of over 500 compared to DAMAS at comparable results.

*Written by Stefan Haxter* (*stefan.haxter@dlr.de*), *DLR, Germany.*

## 7. Miscellaneous

### 7.1. Nonlinear transfer impedance of micro-perforated plates

Micro-perforated plates introduced by Maa [31] are efficient sound absorbers whose application areas vary from room acoustics to duct acoustics. Although there are accurate models for the linear [45] and strongly nonlinear acoustic behavior of MPPs, the transition from one to another has not been a focus of interest so far. A series of measurements are performed with MPP samples for various excitation amplitudes. The deviation from the linear impedance is found to be a function of excitation amplitude and oscillating viscous boundary layer thickness, expressed in terms of the Strouhal number *Sr* and the Shear number *Sh*. Typical for MPPs is a Shear number of order unity, implying that the viscous boundary layer thickness is in the order of the perforation radius. A practical description (in terms of *Sr* and *Sh*) of the transitional behavior of micro-perforated plates (MPPs) has been obtained for conditions between the linear and strongly nonlinear regimes [46]. Using the measurement data, expressions are proposed for calculating the nonlinear acoustic resistance and reactance for circular perforations with sharp square edges. Some additional data is provided for the higher Shear number range such as found in tone-holes of musical instruments. The behavior at low amplitudes for high Shear numbers deviates strongly from the typical MPP behavior. This is due to local vortex shedding at the sharp edges of the perforation as observed already by Ingard and Labatte [23]. These local vortices are probably washed out by viscous dissipation for Shear numbers of order unity. This drastically simplifies the nonlinear behavior of MPPs compared to that of larger orifices.

*Written by Muttalip Askin Temiz* (*muttalip.temiz@gmail.com*), *Ines Lopez Arteaga, Avraham Hirschberg, TU/e, The Netherlands.*

## References

[1] H. Arbey, J. Bataille, Noise generated by airfoil profiles placed in a uniform laminar flow, *Journal of Fluid Mechanics* 134 (33–47) (1983) 9.
[2] Gareth J. Bennett, John A. Fitzpatrick, Noise-source identification for ducted fan systems, *AIAA Journal* 46 (7) (2008) 1663–1674.
[3] Thomas F. Brooks, William M. Humphreys, A deconvolution approach for the mapping of acoustic sources (DAMAS) determined from phased microphone arrays, *Journal of Sound and Vibration* 294 (4–5) (2006) 856–879.
[4] André V.G. Cavalieri, Peter Jordan, William R. Wolf, Yves Gervais, Scattering of wavepackets by a flat plate in the vicinity of a turbulent jet, *Journal of Sound and Vibration* 333 (24) (2014) 6516–6531.
[5] E. Ciappi, F. Magionesi, S. De Rosa, F. Franco, Hydrodynamic and hydroelastic analyses of a plate excited by the turbulent boundary layer, *Journal of Fluids and Structures* 25 (2) (2009) 321–342.
[6] G.M. Corcos, Resolution of pressure in turbulence, *Journal of the Acoustical Society of America* 35 (1963) 192–199.
[7] Ian Davis, Gareth J. Bennett, Experimental investigations of coherence based noise source identification techniques for turbomachinery applications-classic and novel techniques, *17th AIAA/CEAS Aeroacoustics Conference*, 2830, 2011.
[8] Ian Davis, Gareth J. Bennett, Novel noise-source-identification technique combining acoustic modal analysis and a coherence-based noise-source-identification method, *AIAA Journal* 53 (10) (2015) 3088–3101.
[9] Ian Davis, Gareth J. Bennett, Spectral, modal and coherence analysis of sum and difference scattering of narrowband noise in turbomachinery, *International Journal of Aeroacoustics* (2016). in press, http://dx.doi.org/10.1177/1475472X16630860.
[10] S. Deck, Recent improvements in the zonal detached eddy simulation (zdes) formulation, *Theoretical and Computational Fluid Dynamics* 26 (6) (2012) 523–550.
[11] W. Dobrzynski, Almost 40 years of airframe noise research: *what did we achieve? Journal of Aircraft* 47 (2) (2010) 353–367.
[12] Robert P. Dougherty, Extensions of damas and benefits and limitations of deconvolution in beamforming, *11st AIAA/CEAS Aeroacoustics Conference*, 2961, 2005.
[13] Daniel Ernst, Carsten Spehr, Tobias Berkefeld, Decorrelation of acoustic wave propagation through the shear layer in open jet wind tunnel, *21st AIAA/CEAS Aeroacoustics Conference*, 2976, 2015.

[14] R. Ewert, J. Dierke, J. Siebert, A. Neifeld, C. Appel, M. Siefert, O. Kornow, CAA broadband noise prediction for aeroacoustic design, *Journal of Sound and Vibration* 330 (17) (2011) 4139–4160.
[15] Roland Ewert, Juergen Dierke, Andrej Neifeld, S.M. Alavi Moghadam, Linear-and non-linear perturbation equations with relaxation source terms for forced eddy simulation of aeroacoustic sound generation, *20th AIAA/CEAS Aeroacoustics Conference*, 3053, 2014.
[16] F. Franco, S. De Rosa, E. Ciappi, Numerical approximations on the predictive responses of plates under stochastic and convective loads, *Journal of Fluids and Structures* 42 (2013) 296–312.
[17] Michael Goody, Empirical spectral model of surface pressure fluctuations, *AIAA Journal* 42 (9) (2004) 1788–1794.
[18] W.R. Graham, A comparison of models for the wavenumber-frequency spectrum of turbulent boundary layer pressures, *Journal of Sound and Vibration* 206 (4) (1997) 541–565.
[19] S. Haxter, Extended version: improving the damas2 results for wavenumber-space beamforming, *Proceedings of the 6th Berlin Beamforming Conference (BeBeC)*, 2016.
[20] Florian Hindenlang, Gregor J. Gassner, Christoph Altmann, Andrea Beck, Marc Staudenmaier, Claus-Dieter Munz, Explicit discontinuous Galerkin methods for unsteady problems, *Computers and Fluids* 61 (2012) 86–93.
[21] Roger W. Hockney, James W. Eastwood, *Computer Simulation Using Particles*, Taylor & Francis, Inc.,, New York, London, 1988.
[22] N. Hu, C. Appel, M. Herr, N. Rieche, R. Ewert, Numerical study of wall pressure fluctuations for zero and non-zero pressure gradient turbulent boundary layers, *22nd AIAA/CEAS Aeroacoustics Conference*, 2016.
[23] U. Ingård, S. Labate, Acoustic circulation effects and the nonlinear impedance of orifices, *The Journal of the Acoustical Society of America* 22 (2) (1950) 211–218.
[24] Don H. Johnson, Dan E. Dudgeon, *Array Signal Processing: Concepts and Techniques*, Prentice Hall, Upper Saddle River, New Jersey, 1993.
[25] Lloyd E. Jones, Richard D. Sandberg, Numerical analysis of tonal airfoil self-noise and acoustic feedback-loops, *Journal of Sound and Vibration* 330 (25) (2011) 6137–6152.
[26] Jae Wook Kim, Sina Haeri, An advanced synthetic eddy method for the computation of aerofoil–turbulence interaction noise, *Journal of Computational Physics* 287 (2015) 1–17.
[27] Jae Wook Kim, Sina Haeri, Phillip F. Joseph, On the reduction of aerofoil–turbulence interaction noise associated with wavy leading edges, *Journal of Fluid Mechanics* 792 (526–552) (2016) 4.
[28] Alexander Klabes, Christina Appel, Michaela Herr, Mohamed Bouhaj, Fuselage excitation during cruise flight conditions: measurement and prediction of pressure point spectra, *21st AIAA/CEAS Aeroacoustics Conference*, 2015.
[29] Alex S.H. Lau, Sina Haeri, Jae Wook Kim, The effect of wavy leading edges on aerofoil–gust interaction noise, *Journal of Sound and Vibration* 332 (24) (2013) 6234–6253.
[30] J.H. Lin, Y.H. Zhang, Y. Zhao, Pseudo excitation method and some recent developments, *Procedia Engineering* 14 (2011) 2453–2458.
[31] Dah-You Maa, Potential of microperforated panel absorber, *The Journal of the Acoustical Society of America* 104 (5) (1998) 2861–2866.
[32] Eric Manoha, Jean Bulté, Vlad Ciobaca, Bastien Caruelle, Lagoon: further analysis of aerodynamic experiments and early aeroacoustics results,*15th AIAA/CEAS Aeroacoustics Conference*, 3277, 2009.
[33] S. Narayanan, P. Chaitanya, S. Haeri, Phillip F. Joseph, J.W. Kim, C. Polacsek, Airfoil noise reductions through leading edge serrations, *Physics of Fluids* 27 (2) (2015) 025109.
[34] Andrej Neifeld, Dirk Boenke, Juergen Dierke, Roland Ewert, Jet noise prediction with eddy relaxation source model, *21st AIAA/CEAS Aeroacoustics Conference*, 2370, 2015.
[35] S. Oerlemans, C. Sandu, N. Molin, J.-F. Piet, Reduction of landing gear noise using meshes, *16th AIAA/CEAS Aeroacoustics Conference*, 2010.
[36] Léo S. Pires, Robert P. Dougherty, Samir N.Y. Gerges, Fernando Catalano, Predicting turbulent decorrelation in acoustic phased array, *50th AIAA Aerospace Sciences Meeting including the New Horizons Forum and Aerospace Exposition*, 387, 2012.
[37] B. Plogmann, A. Herrig, W. Würz, Experimental investigations of a trailing edge noise feedback mechanism on a naca 0012 airfoil, *Experiments in Fluids* 54 (5) (2013) 1–14.
[38] Cyril Polacsek, Virginie Bonneau, Lionel Castillon, Julien Marty, Mathieu Gruber, Turbofan broadband noise predictions using a 3D zdes rotor blade simulation, *Proceedings of INTER-NOISE 2015*, Institute of Noise Control Engineering, San Francisco, 2015.
[39] G. Reboul, C. Polacsek, S. Lewy, S. Heib, Ducted-fan broadband noise simulations using unsteady or averaged data, *Proceedings of the INTER-NOISE 2008*, Institute of Noise Control Engineering, Shanghai, China, 2008.
[40] S. Redonnet, G. Cunha, An advanced hybrid method for the acoustic prediction, *Advances in Engineering Software* 88 (2015) 30–52.
[41] Stéphane Redonnet, Guilherme Cunha, S. Ben Khelil, Numerical simulation of landing gear noise via weakly coupled CFD-CAA calculations, *19th AIAA/CEAS Aeroacoustics Conference*, 2068, 2013.
[42] Stéphane Redonnet, David P. Lockard, Mehdi R. Khorrami, Meelan M. Choudhari, The non-reflective interface: *an innovative forcing technique for computational acoustic hybrid methods*, *International Journal for Numerical Methods in Fluids* 81 (1) (2016) 22–44.
[43] T. Rougier, Q Bouvy, D. Casalino, J. Appelbaum, C. Kleinclaus, Design of quieter landing gears through lattice-Boltzmann cfd simulations, *21st AIAA/CEAS Aeroacoustics Conference*, 2015.
[44] Carsten Spehr, Holger Hennings, Heino Buchholz, Mohamed Bouhaj, Stefan Haxter, Anne Hebler, In-flight sound measurements: a first overview, *Proceedings of the 18th AIAA/CEAS Aeroacoustics Conference*, 2012.
[45] Muttalip Askin Temiz, Ines Lopez Arteaga, Gunilla Efraimsson, Mats Åbom, Avraham Hirschberg, The influence of edge geometry on end-correction coefficients in micro perforated plates, *The Journal of the Acoustical Society of America* 138 (6) (2015) 3668–3677.
[46] Muttalip Askin Temiz, Jonathan Tournadre, Ines Lopez Arteaga, Avraham Hirschberg, Non-linear acoustic transfer impedance of micro-perforated plates with circular orifices, *Journal of Sound and Vibration* 366 (2016) 418–428.
[47] J.C. Tyacke, M. Mahak, P.G. Tucker, Large-scale multifidelity, multiphysics, hybrid Reynolds-averaged Navier–Stokes/large-eddy simulation of an installed aeroengine, *Journal of Propulsion and Power* 32 (4) (2016) 997–1008, http://dx.doi.org/10.2514/1.B35947.